Quantum optics and quantum computing experimental-toolkit for education and research: Learning quantum science & technologies by doing

PsiQuanTech Private Limited, Bengaluru South-562138.

I. INTRODUCTION AND MOTIVATION

Quantum technologies (the future technology) viz., quantum computation and communication, quantum metrology and sensing, and quantum materials and devices, are emerging at an unprecedented rate. Indian government has sanctioned 6003 crore INR (726 million USD) to boost the quantum technology based industries, in the coming seven years (https://dst.gov.in/national-quantum-mission-nqm) and government of Andhra Pradesh is constructing the Amaravati Quantum Valley. Global investment for quantum computing alone is 55 billion USD. Global market which the quantum-gravimeter alone can address is 71 trillion USD [23]. Many Nobel prizes are being awarded for fundamental breakthroughs which are opening up the doors to new quantum technologies e.g., 1997 and 2001 Nobel prizes were awarded to laser cooling-and-trapping of atoms and Bose-Einstein condensate (BEC) respectively which have lead to the possibility of highly sensitive quantum-gravimeter [23] and quantum inertial navigation system (10^{11} times more sensitive than the classical laser-based gyroscope [14]) [10], trapped atom/ion quantum computing (e.g., it takes 10000 years for a state-of-the-art classical supercomputer to do a certain task which a quantum computer can do in just 200 seconds [1]), highly precise and stable atomic clocks (less than one second error in time-keeping over 50 million years [4]) etc. And 2022 Nobel prize was awarded for breakthroughs in quantum information and communication.

Hence it is important and also necessary to train the students (with hands on experience) in quantum technologies, so that they can be the leaders/architects of the future technology. (Please note that many of the current technologies based on classical principles are going to become obsolete soon.) For this purpose, we will be happy to build and supply affordable compact experimental quantum technologies toolkits for B.E/B.Tech, M.Tech, BSc and MSc student's laboratory and also for R & D labs.

Quantum mechanics not only has technological significance but also has fundamental significance e.g., consider quantum entanglement and nonlocality which is an experimentally well established fact [12, 19]. It has baffled scientists since it was first pointed out by Einstein in his famous EPR paradox [8] and later exaggerated by Schrödinger in his famous cat paradox [13]. Quantum nonlocality appears to be the basis of the entire physical world (for its likely connection to Advaitha (non-dual) philosophy see [21, 22]). A deeper understanding of the foundations of quantum mechanics may give rise to newer and much more powerful quantum technologies e.g., see [22].

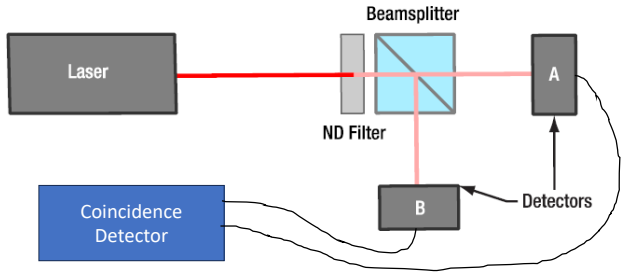

FIG. 1. Schematic of the HBT experimental setup with attenuated laser.

II. QOC-QUANTUM OPTICS CORE TOOLKIT

Using the quantum optics core-toolkit (QOC), students can perform the following experiments.

A. Hanbury-Brown-Twiss experiment with attenuated laser: Classical-light source

Goal: Test whether an attenuated laser is a suitable single photon (quantized light) source, using Hanbury-Brown-Twiss (HBT) experimental setup.

Setup: The laser is attenuated by a neutral density (ND) filter and then hits a beamsplitter. The single photon detectors A and B are placed in the output ports of the beamsplitter (see Fig. 1).

Result Analysis: The second-order cross-correlation function $g^{(2)}_{HBT}(\tau)$ can be calculated via the following equation [6]:

$$g^{(2)}_{HBT}(\tau) = \frac{R_{AB}(t, t+\tau)}{R_A(t+\tau).R_B(t).\Delta t} = \frac{\langle I_A(t+\tau).I_B(t)\rangle}{\langle I_A(t+\tau)\rangle.\langle I_B(t)\rangle} \quad (1)$$

where $R_A(t'), R_B(t')$ are the average count rates of the detectors A, B respectively at time t', and $R_{AB}(t, t+\tau)$ is the average count rate of two detection events which are separated in time by τ seconds (for $\tau = 0$ this becomes the coincidence count rate at time t), Δt is the time window of a given detection event typically a few ns, and $\langle I_A(t')\rangle$ is the expectation value of the intensity of light at time t' as measured by detector A. Taking $\tau = 0$ we

get [6]:

$$(1/\Delta t)\int_{\Delta t} g^{(2)}_{HBT}(\tau)d\tau \approx g^{(2)}_{HBT}(0) = \frac{R_{AB}(0)}{R_A.R_B.\Delta t}. \quad (2)$$

This function is called "second order" because it describes the correlation of intensities. A first-order correlation function indicates correlations between amplitudes. With a single photon source in Fig. 1, we should get $g^{(2)}_{HBT}(0) \ll 1$ (anti-coincidence). However using the setup in Fig. 1, we will get $g^{(2)}_{HBT}(0) \approx 1$ (this corresponds to $\langle I_A(t).I_B(t)\rangle \approx \langle I_A(t)\rangle.\langle I_B(t)\rangle$) indicating that the laser is an uncorrelated classical light source (this is true even for an highly attenuated (via ND filters) laser beam). This is because even an highly attenuated laser beam consists of bunches of photons (because two identical Bosons can occupy the same given quantum state with all quantum numbers same, unlike Fermions) but not single photons which are separated in space and time. In fact, laser light is quantum mechanically represented by a coherent state for which the photon statistics is a Poisson distribution (this corresponds to completely random i.e., g2(0)=1, light source). Irrespective of the attenuation, the laser always emits multiple photons often enough to make $g^{(2)}_{HBT}(0) \approx 1$, as expected. Simply attenuating the laser does not change the underlying statistics of the light. Note that in the experiment here, the laser is attenuated both before and after the beamsplitter due to the bandpass filters in front of the detectors. Ideally, the attenuation would take place only before the beamsplitter.

Sample experimental measurement readings (taken from elsewhere) are given in Table I.

Parameter	Measured value
Δt	5 ns
R_A	391118.45 Hz
R_B	315945.65 Hz
R_{AB}	619.1 Hz
$g^{(2)}_{HBT}(0)$	1.00201

TABLE I. Sample experimental measurement readings for HBT experiment with attenuated laser.

B. HBT experiment with a BBO nonlinear crystal: Quantum-light source (heralded single photon pairs)

Goal: Test whether the source is indeed emitting photon pairs i.e., heralded single photons.

Setup: The 405 nm pump laser is down converted into 810 nm photon pairs (via spontaneous parametric down conversion (SPDC)) in the $\beta - BaB_2O_4$ i.e., beta-Barium borate (BBO) nonlinear crystal. One single photon detector is placed in each path, as shown in Fig. 2.

Measurement: Darken the room, and start the laser. Record the count rates for detectors T and A and their coincidence count rate.

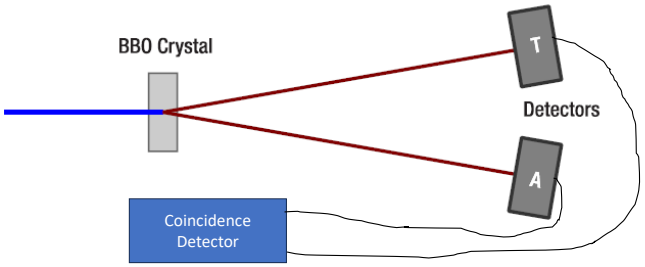

FIG. 2. Schematic of the HBT experimental setup to test if the source is indeed emitting single-photon pairs.

Result Analysis: Here we should obtain

$$g^{(2)}_{HBT}(0) = \frac{R_{AT}(0)}{R_A.R_T.\Delta t} \gg 1 \quad (3)$$

if the source is a single photon source.

Interpretation: For completely uncorrelated light, one would expect the coincidences to be completely random, resulting in a $g^{(2)}_{HBT}(0)$ value of 1. However, due to the photon pairs generated by the BBO crystal, there are many more coincidences than what would be expected in the random case. The value of $g^{(2)}_{HBT}(0)$ is the factor between the measured and expected coincidences and should be at least 30 in the measurement you take. Such a large $g^{(2)}_{HBT}(0)$ proves the generation of photon pairs.

C. HBT Experiment with only one arm of the single photon pair source

Goal: Test if one arm of the photon pair source is a single photon source.

Setup: Place a beam-splitter in one of the detection arms and place single photon detectors at both outputs of the beam-splitter, as shown in Fig. 3. Then block the arm leading to detector T using a beam blocker.

Result analysis: Here the correlation is measured using the relation

$$g^{(2)}_{HBT}(0) = \frac{R_{AB}(0)}{R_A.R_B.\Delta t}. \quad (4)$$

Interpretation: A single arm of the photon pair source is not a single photon source. The photons are actually in a thermal state (whose statistics is described by Bose-Einstein distribution), so one would expect $g^{(2)}_{HBT}(0) = 2$ with ideal detectors. However, as the time resolution of the detectors used here is far too low and integration leads to the result $g^{(2)}_{HBT}(0) = 1$. Hence

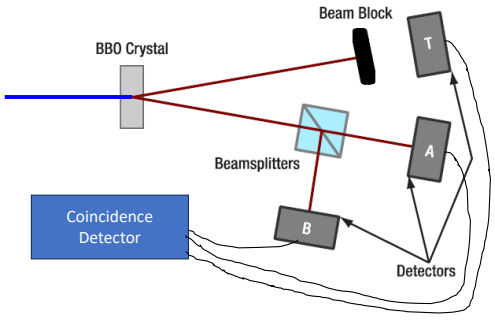

FIG. 3. Schematic of the setup to test if only one arm of the photon pair source is a single photon source.

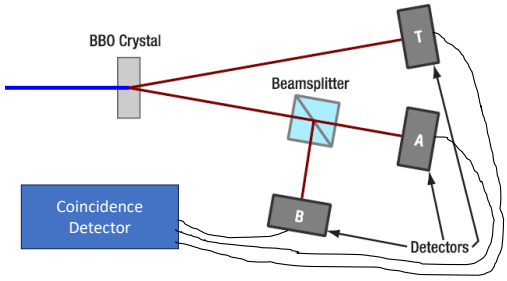

FIG. 4. Schematic Setup to test whether the pair source is a single photon source when counts are measured only in coincidence with the trigger detector.

here we will obtain $g^{(2)}_{HBT}(0) \approx 1$, indicating that a single arm of the photon pair source is not a single photon source (if it were single photons then we should have got $g^{(2)}_{HBT}(0) \ll 1$ (anti-coincidence)). To perform single photon experiments with a pair source, one must use the information of the second photon of a pair to create a single photon state, which is shown in the next experiment.

D. Grangier-Roger-Aspect (GRA) Experiment: Photon triple coincidence and heralded single photons

Goal: Test whether the pair source is a single photon source when counts are measured only in coincidence with the trigger detector.

Setup: See Fig. 4.

Sample experimental measurement readings (taken from elsewhere) are given in Table II.

Result analysis: Calculate the correlation using the relation

$$g^{(2)}_{GRA}(0) = \frac{R_{TAB}(0).R_T}{R_{TA}.R_{TB}} \tag{5}$$

where R_{TAB} is the triple coincidence count rate.

Interpretation: For classical light, one would expect a certain number of random triple coincidences depending on the number of trigger events, resulting in a $g^{(2)}(0)$ value between 1 and 2. However, the experiment results in $g^{(2)}_{GRA}(0)$ have values much lower than 1, proving that we are dealing with a non-classical light source. Note that the expectation value of $g^{(2)}_{GRA}(0)$ does not depend on the measurement time. The standard deviation on the other hand can be reduced by longer measurement times. Further note that if we perform GRA experiment with classical light source (i.e., remove BBO crystal and put a fluorescent filter which scatters the light in all directions) then we obtain $g^{(2)}_{GRA}(0) \approx 1$, as shown in the next experiment.

Parameter	Measured value
Total measurement time	20 s
Total Counts (detector T)	4638000
Total Counts (detector A)	2905000
Total Counts (detector B)	2925000
Total coincidence counts (T&A)	385865
Total coincidence counts (T&B)	324688
Total coincidence counts (T&A&B)	513
$g^{(2)}_{TA}(0)$-Correlation T&A with $\Delta t = 5ns$	114.56
$g^{(2)}_{GRA}(0)$-Correlation A&B triggered by T	0.0190

TABLE II. Sample experimental measurement readings for GRA experiment. Here $g^{(2)}_{TA}(0) = \frac{R_{TA}(0)}{R_A.R_T.\Delta t}$ and $g^{(2)}_{GRA}(0)$ is given by Eq. (5).

E. GRA Experiment with Classical Light

Goal: Perform the GRA experiment with a non-pair classical light source.

Setup: Use the setup of previous experiment and replace the BBO crystal with the fluorescent filter. The filter will emit fluorescent light in all directions, so that you can perform the GRA experiment with it. A schematic of the setup is shown in Fig. 5.

Measurement: Darken the room, set the laser current to about 5 mA below the lasing threshold (check the spec sheet of your laser diode), then perform the GRA experiment 10 times with 20 s measurement time for each.

Result Analysis: The results are generated with the same formula as earlier i.e.,

$$g^{(2)}_{GRA}(0) = \frac{R_{TAB}(0).R_T}{R_{TA}.R_{TB}}. \tag{6}$$

However, this time, the result will always be close to 1.

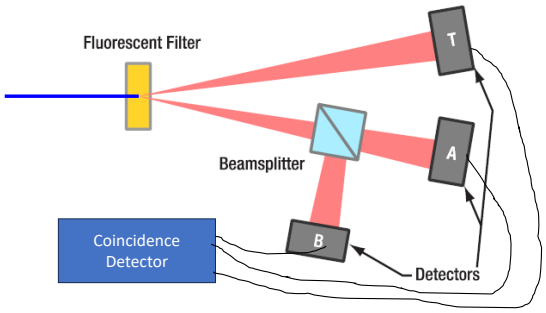

FIG. 5. Schematic of GRA experimental setup with classical non-pair light source.

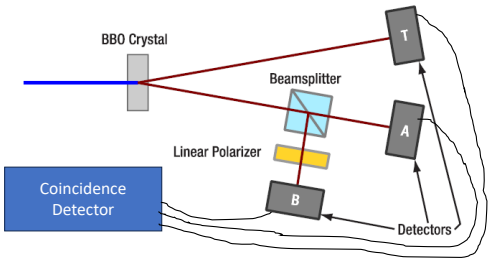

FIG. 6. Schematic of the setup to demonstrate Malus' law with single photons.

Interpretation: The light from the filter is in a thermal state. The fluorescent photons are not generated as entangled pairs but randomly. Thus, there is no correlation between events on detector T and detectors A and B. And hence each term in the above relation factors out into product of individual detector click rates (this is easily seen if we express R's in terms of intensities). Consequently in this case the triple coincidence detection scheme produces the same result as the simpler HBT experiment with classical light i.e., $g^{(2)}(0) = 1$. This proves that the result measured in Sec. II D was not generated only by the change of the detection scheme, but that a pair photon source is required to be able to generate single photon states this way.

F. Malus' law for single photons: Demonstrating the wave nature exhibited even by single photons

Goal: Test the polarization properties of single photons.

Setup: Take the setup from Sec. II D and place a rotatable linear polarizer between the beamsplitter and detector, as shown in Fig. 6.

Measurement: Set the polarizer to 0°. Darken the room and record a measurement with measurement time 20 s (the important data points here are $g^{(2)}_{GRA}(0)$ and R_{TB}). Then rotate the polarizer by 10° and repeat the measurement. Record measurements in 10° steps between 0° and 180° (or 360° for a larger data set).

Result analysis: Plot the coincidence count rate R_{TB} and the correlation $g^{(2)}_{GRA}(0)$ over the polarizer angle. You will obtain

$$R_{TB} = R^{max}_{TB} \cos^2(\theta - \phi) \tag{7}$$

where ϕ being the polarization angle of the single photons, and θ is the polarizer angle with respect to a reference vertical axis. Note that due to the process of generating the photon pairs, the polarization in both arms of the pair photon source is expected to be parallel. This can be verified by positioning the polarizer in front of detector T instead of B and repeating the experiment.

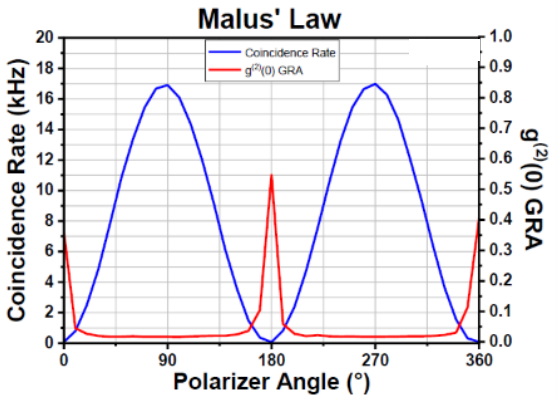

FIG. 7. Sample experimental measurement readings (taken from elsewhere) for the Malu's law with single photons. Here the vertical axis on the left side is R_{TB}. The simultaneously measured correlation values $g^{(2)}_{GRA}(0)$ are always well below 1, showing that the experiments were always in the single photon regime. The higher values for $g^{(2)}_{GRA}(0)$ at $0^o, 180^o, 360^o$ are a result of the extremely low count rates at those angles, significantly increasing the noise and the contribution of uncorrelated stray light to the signal.

Sample experimental measurement readings: See Fig. 7.

Interpretation: The coincidence count rate shows a $\sin^2$-dependence on the polarizer angle. This is known as Malus' law. However, the simultaneously measured correlation values $g^{(2)}_{GRA}(0)$ are always well below 1, showing that the experiments were always in the single photon regime. The higher values for $g^{(2)}_{GRA}(0)$ at $0^o, 180^o, 360^o$ are a result of the extremely low count rates at those angles, significantly increasing the noise and the contribution of uncorrelated stray light to the signal. In summary, the experiment shows that single photons can pass

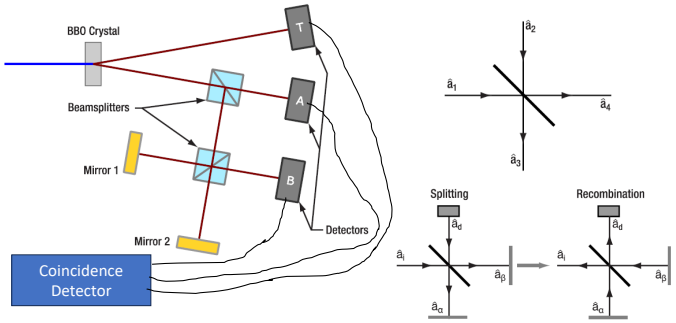

FIG. 8. Schematic diagram of the setup of single photon Michelson interferometer. Here mirror-1 is kept on a moving stage to introduce path length difference of Δl.

through a linear polarizer and that their probability to do so shows the same behavior as the intensity of a classical electromagnetic wave.

G. Single Photon Michelson Interferometer: Demonstrating the wave nature exhibited even by single photons

Goal: Test the interference (with itself) property of a single photon and determine its wavelength (this requires an ensemble of single photons).

Setup: Setup the experiment as shown in Fig. 8.

Theory: Quantum Mechanical Treatment of a beam splitter: Consider a lossless beam splitter with the geometry shown in Fig. 8, with $\hat{a}_1, \hat{a}_2$ being the annihilation operators of the input ports and $\hat{a}_3, \hat{a}_4$ being the annihilation operators of the output ports. With the transmission and reflection coefficients of the beam splitter being t and r respectively, it can be shown [3] that the following relations hold for the annihilation and creation $(\hat{a}_j^\dagger, j = 1, 2, 3, 4)$ operators of the ports:

$$\hat{a}_1 = r.\hat{a}_3 + t.\hat{a}_4, \hat{a}_2 = t.\hat{a}_3 - r.\hat{a}_4,$$
$$\hat{a}_1^\dagger = r.\hat{a}_3^\dagger + t.\hat{a}_4^\dagger, \hat{a}_2^\dagger = t.\hat{a}_3^\dagger - r.\hat{a}_4^\dagger. \quad (8)$$

Consider the input mode $|1\rangle_1|0\rangle_2$, i.e., a Fock state with a photon number of 1 at input port 1 and the quantized electromagnetic field vacuum state at input port 2 (a single photon incident on the beamsplitter at port 1). Let $t = r = 1/\sqrt{2}$ i.e., 50:50 beamsplitter. Then using Eqs. (8) we obtain,

$$|1\rangle_1|0\rangle_2 = \hat{a}_1^\dagger|0\rangle_1|0\rangle_2 = (|1\rangle_3|0\rangle_4 + e^{i\phi}|0\rangle_3|1\rangle_4)/\sqrt{2} \quad (9)$$

where the phase shift $\phi = 2\pi\Delta l/\lambda$ depends on the path length difference Δl between the two paths/arms of the interferometer and λ is the wavelength associated with the single photon. Similar calculations give the state after the second beam splitter (i.e., after recombination) to

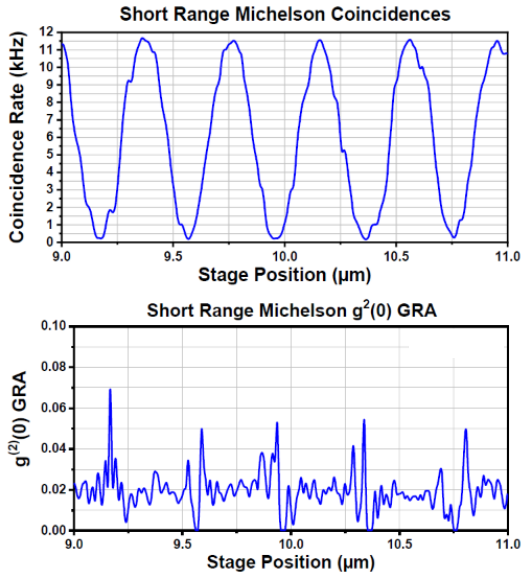

FIG. 9. Sample experimental measurement readings (taken from elsewhere) for the single photon Michelson interferometer. Here the vertical axis in the top plot is R_{TB}. The simultaneously measured correlation values $g^{(2)}_{GRA}(0)$ are always well below 1, showing that the experiments were always in the single photon regime. Here time per Data Point is 1200 ms.

be

$$((1 + e^{i\phi})|1\rangle_i|0\rangle_d + (1 - e^{i\phi})|0\rangle_i|1\rangle_d)/2 \quad (10)$$

where i, d denote incident and detector ports respectively. From the state (10) we obtain the probability for finding the single photon in the port-d and port-i to be $(1 - \cos\phi)/2$ and $(1 + \cos\phi)/2$ respectively. Hence quantum mechanics predicts the wave nature exhibited even by a single photon.

Measurement: Darken the room and start a measurement with a long range of stage positions (for example $2 - 8\mu m$), a short integration time (such as 300 ms) and a medium step width (such as 75 nm). Measurement should correspond to evaluating $g^{(2)}_{GRA}(0)$ and

$$R_{TB} = R^{max}_{TB}(1 + \cos(2\pi\Delta l/\lambda))/2 \quad (11)$$

[9], and then plot these over mirror stage position.

Carryout a second measurement, this time with a reduced measurement range (for example $9\mu m$ start position and $11\mu m$ end position), a longer integration time (such as 1200 ms), and a smaller step width (such as $50nm$).

Sample experimental measurement readings: See Fig. 9.

Result Analysis: Determine the average spacing between two consecutive maxima $(\Delta l')$ in the plot and calculate the wavelength of the single photons using the

relation $\Delta\phi' = 2\pi\Delta l'/\lambda$ where $\Delta\phi' = \pi$. E.g., in the sample measurement in Fig. 9, $\Delta l' \approx 0.4\mu m$ which gives $\lambda = 800nm$. Another method is the following: By moving the mirror over a length l and counting the number N of maxima during this movement, the wavelength of the photons can be determined using the relation $\lambda = 2l/N$.

Interpretation: The first measurement shows the interferogram over nearly the entire range of the interferometer. The interferogram resembles a sine/cosine curve (as predicted by Eq. (11)). The maxima will be evenly spaced, and the wavelength calculation should result in a value close to 810 nm (twice the pump laser wavelength), with an error of up to 3% due to the accuracy of the stage position control. The amplitude of the interference should not change significantly over the whole measurement range, pointing to a coherence length of the photons larger than 20 μm. However quantitatively determining the coherence length requires additional measurements, as discussed in Sec. III.

The $g^{(2)}_{GRA}(0)$ graph of the first measurement may show significant noise. For some data points $g^{(2)}_{GRA}(0)$ may measure as 0 but may reach up to 0.15 at some points. The reason for this behavior is the short measurement time per data point. As the calculation of $g^{(2)}_{GRA}(0)$ is highly sensitive to the number of triple coincidences, and those occur at a much lower rate than two-detector coincidences, more time is required to get meaningful values. However, the average $g^{(2)}_{GRA}(0)$ is still well below 1, pointing to the single photon regime.

For the second measurement, a larger time per data point and a smaller measurement range were used. As a result of the increased time per data point, the noise of the $g^{(2)}_{GRA}(0)$ curve will be significantly lower than for the first measurement. The value of this function is always below 0.1, clearly proving that the whole measurement was performed with non-classical light. Around the minima of the interferogram, all coincidence count rates are much lower. This results in higher noise and a higher relative contribution of uncorrelated stray light to the signal for the $g^{(2)}_{GRA}(0)$ values of these data points.

H. Quantum erasure experiment: Demonstrating wave-particle duality and Bohr's complementarity principle using single photons

Goal: To demonstrate the quantum erasure effect using single photons.

Setup: Consider the setup in Fig. 8 and place one $1/2''$ diameter polarizer in each arm of the Michelson interferometer, as shown in Fig. 10.

Measurement: Set both polarizers 1 and 2 in the setup Fig. 10 to 0°, darken the room. Set the start and end positions of the stage at about $1\mu m$ apart. Record an interferogram measurement by moving the stage in small steps as earlier. Then rotate one of the polarizers 1 or 2 to 90° and record another measurement with the same parameters as before. Now place a linear polarizer-3 set to 45° directly in front of detector B and repeat the previous measurement.

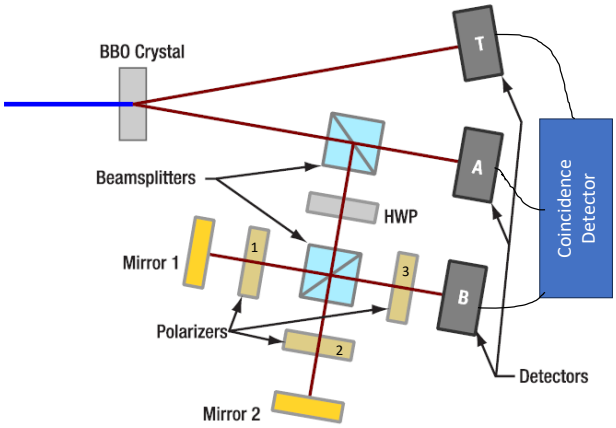

FIG. 10. Schematic setup of the quantum erasure experiment.

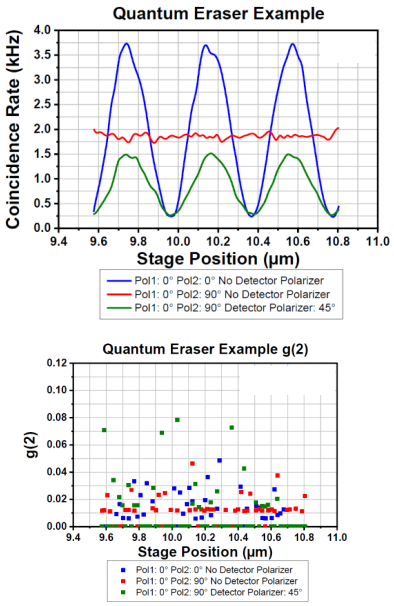

FIG. 11. Sample experimental measurement readings (taken from elsewhere) for the quantum erasure experiment. Here the vertical axis in the top plot is R_{TB}. The simultaneously measured correlation values $g^{(2)}_{GRA}(0)$ are always well below 1, showing that the experiments were always performed in the single photon regime.

Sample experimental measurement readings: See Fig. 11.

Result and interpretation: Plot the R_{TB} coincidence count rate with respect to the stage position for all three measurements in one plot. Create a second plot with the values of the $g^{(2)}(0)$-function as a function of the stage position. The first measurement (both polarizers at 0°) shows a typical interferogram as the polarizations in

both arms are parallel.

In the second measurement, the polarization in the arms is set to be perpendicular to each other. Because it would now be possible to determine which arm the photon took at the position of detector B (via a simple polarization measurement), no interference is observed anymore. The constant coincidence count rate will be about half of the maximum rate of the first measurement. Note that in this case there will be entanglement between spatial and polarization degree(s) of freedom (d.o.f). Hence even if we do not measure the polarization-state to know which path the photon took, still no interference fringes will be observed in spatial d.o.f. This is because, due to entanglement, information will be distributed in the global space of spatial and polarization d.o.f (in this case the reduced state corresponding to spatial d.o.f is mixed which exhibits no/reduced interference).

The information about the path can be "erased" by the 45° polarizer in the third measurement. The probability of a photon reaching the detector is now again the same for both arms, hence an interference curve is observed in the third measurement. The third polarizer is absorbing half of the remaining photons, so the amplitude of the curve in the third measurement will be much lower than that in first measurement. The $g^{(2)}(0)$ function should be below 0.1 for all data points, to make sure that all measurements were in the single photon regime.

Bohr's complementarity principle is a consequence (directly or indirectly) of Heisenberg's uncertainty principle [2, 7, 18]. Hence it shows that we cannot simultaneously observe both wave and particle natures exhibited by a quantum object like photon, by measuring non-commuting observables in the same given experimental arrangement (note that measuring non-commuting observables requires different experimental arrangements). Note that Bohr's complementarity principle associates particle nature to which-path information and wave nature to interference fringe visibility e.g., in quantum-erasure/Young's double-slit experiment. But it is not really necessary to know which-path information to observe particle nature. E.g., in Young's double slit experiment with a single photon/electron, the very fact that we get a single well localized spot on the screen (or a single detector click) itself shows the existence of a particle. As interference fringes develop over many repetitions of the experiment, wave nature must also be associated with the particle, simultaneously. Hence if we can define wave and particle natures of a quantum object using commuting observables, then the same can be observed simultaneously using the same given experimental arrangement and a single measurement outcome [2, 11].

I. Measuring the coherence length

The coherence length l_c of a light source can be determined by evaluating the envelope of the interferogram taken with the source, as shown in Fig. 12. $l_c = \lambda^2/\Delta\lambda$

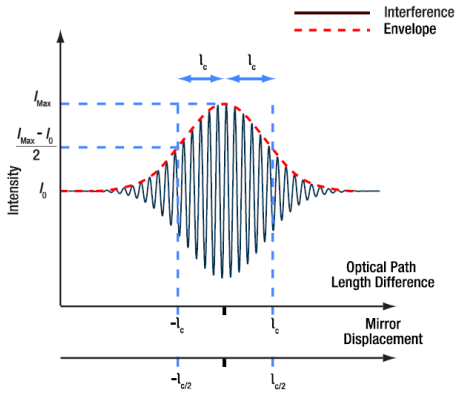

FIG. 12. Determining the coherence length from interferogram

where $\Delta\lambda$ is full width at half maxima (FWHM). The photons generated by the SPDC process in the BBO crystal have $\lambda = 810nm$. The spectral width of the photon wavelength distribution is larger than the window of the bandpass filters in front of the detectors. Hence, $\Delta\lambda = 10nm$ is given by the filter window size. This yields $l_c = 65.6\mu m$.

The coherence length is equal to the FWHM of the envelope when the stage position is plotted on the x-axis. Small side maxima will be caused by the spectral function not being a Gaussian (ideal case) but closer to a rectangle (due to the bandpass filters). For a rectangular spectrum, the envelope is expected to resemble the shape of a $|sinc(x)| = |\sin(x)/x|$ function. Please note that the position of the differential screw can lead to an error of about 10% in the position readings due to the non-linearity of the stage. The least deviation occurs in the center of the travel range of the differential screw.

An additional experiment could be to exchange the bandpass filters in front of all three detectors with filters with a broader window. This way, the coherence lengths would decrease, so that the "true" spectrum of the SPDC source could be measured even with a single interferogram over the whole range of the translation stage. Additionally, the side maxima should disappear due to the spectrum being closer to a Gaussian than to a rectangle.

J. The three polarizer paradox

The three-polarizer-paradox describes a situation where the transmission through two crossed polarizers is zero. Upon adding a third polarizer at 45° rotation (with respect to the polarization axis of the other two polarizers) in between, the intensity increases again. This may be counter-intuitive when thinking about single photons. From a quantum mechanics perspective, there is a chance that a photon gets either absorbed or transmitted at each

polarizer (according to Malus' law).

If there were nothing more to it, the increase of the transmitted signal could not be explained, as adding a third polarizer should only decrease the chance of transmission through all polarizers. But in terms of quantum mechanics, each polarizer must be viewed as a measurement device. As such, the measurement does not just give a reading of the probability to end up in this polarization state, but also projects the incoming state onto the state of the measurement result. Therefore, in the case of two crossed polarizers, the first polarizer projects the state onto its own axis and the second polarizer has zero probability for photons to transmit in this state. But once the third polarizer is introduced in between, the state projected by the first polarizer is measured and projected by the intermediate polarizer again. According to Malus' law, the probability to measure a transmitted photon after the 45° rotated polarizer is 1/2. The last polarizer again measures the probability for the photons projected to the 45° rotated polarization to pass the 90° oriented polarizer, which is also 1/2. Multiplying the probabilities at each polarizer yields 1/4 for the transmission through both polarizers after the first one.

This experiment can be set up with the components in QOC. All three polarizers can be placed in front of detector B and the alignment laser can be used to properly line up the components. To achieve the same height for all three polarizers, you may use the Michelson interferometer breadboard or one spacer for each 1/2" polarizer.

A more detailed analysis of this topic and its implications for teaching can be found in the literature [5], including the optical analogue of the Stern-Gerlach experiment.

K. Elitzur-Vaidman bomb tester: Detecting a bomb without exploding it

For convenience, instead of a bomb let us place a single-photon detector D_3 in path-2 of the Mach-Zehnder interferometer (MZI) as shown in Fig. 13 (b). Then a single photon interacts with D3 and their combined state after interaction is given by $|1\rangle_1|D3\rangle + |0\rangle_2|D3'\rangle$ where $|D3'\rangle$ represents state of the detector D3 after absorbing a photon. Hence when the outcome corresponding to D3 not clicking is realized, the photon goes through path-1 (within standard quantum mechanics this corresponds to D3 inducing collapse of the wave function to the state $|1\rangle_1|D3\rangle$) and consequently no interference will be observed after the second beam splitter in MZI (i.e., there will be non-zero probability for both detectors D_1, D_2 clicking). This corresponds to the case in which a live bomb is detected without exploding it. This clearly shows that calling this as an "interaction-free" measurement is a misleading terminology. Without interaction between photon and D3, there can be no entanglement between various possible states of photon and D3 which is demanded-by/follows-from the linearity of Schrödinger equation. This experiment can be realized using the components included in QOC.

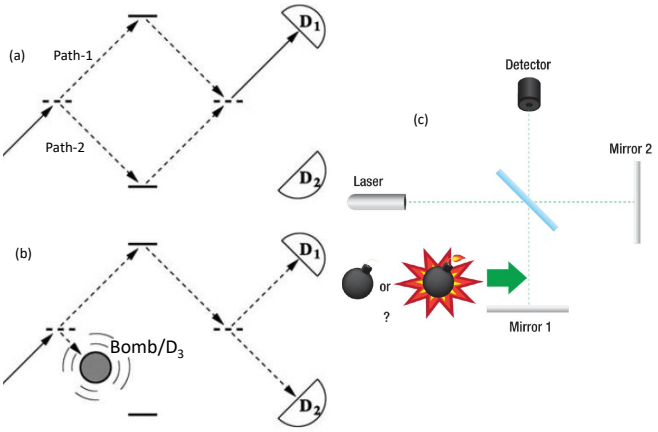

FIG. 13. Schematic of the bomb-tester experiment in (a,b) MZI setup and (c) Michelson interferometer setup (this can be realized using the components included in QOC).

L. Demonstrating spatial correlation of the photon pairs

A simple experiment can highlight the spatial correlation of the photon pairs. The two photons of a pair are located at opposite sides of a cone surface originating at the BBO crystal. Thus, if one photon of a pair arrives on the lower half of the aperture of detector T, the other photon is expected to arrive at the upper half of the aperture on detector A, as sketched in Fig. 14.

This can be tested by blocking the upper/lower half of the detector apertures of T and A and recording the single detector count rates as well as the T&A coincidence count rate for all four combinations. The coincidence rate should be much higher for the up-down and down-up combinations (photons of a pair are either both blocked or both pass) than for up-up and down-down (for every pair, only one photon can pass), while the single detector count rates remain stable.

M. Direct event pulse observation

For educational purposes one may want to view the TTL pulses generated by the three detectors directly. Observing the incoming pulses can be helpful to establishing an understanding of the different temporal distribution for the pair source compared to a classical light source. Based on these observations the statistical quantities described earlier can be motivated further. Viewing the pulses directly also helps when discussing technical aspects of the detectors, like pulse length, jitter, or afterpulsing.

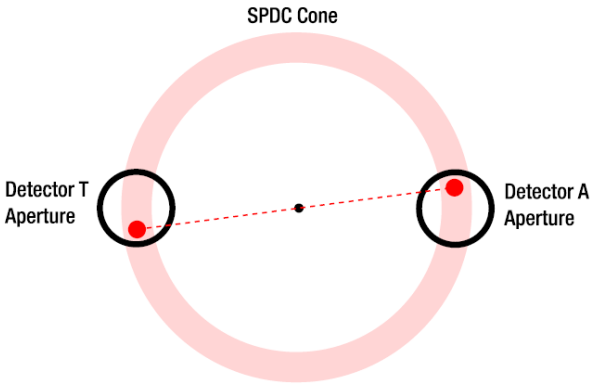

FIG. 14. Sketch of the spatial correlation of photon pairs. The red dots mark photons of one pair.

To view the detector pulses, you can use any kind of oscilloscope or logic level analyzer with a timing resolution on the order of nanoseconds, i.e., a minimum bandwidth of about 1 GHz.

Recommended general settings for any kind of scope are: A displayed time window of 200 - 500 nanoseconds, A maximum voltage level of 5 V, A trigger level at 0.5 - 2 V, A negative trigger delay of a few 10s of nanoseconds, to show what happens before the trigger pulse arrives, Trigger input on pulses of detector T.

You may choose to trigger on detectors A or B instead as well. However, triggering on detector T will show similar relative frequencies of coincidence events as in the experiments described above. As the detection rates on detector T are highest (while A or B have at maximum half the rate due to the beamsplitter), many trigger events will only show a trigger pulse without coincidence. Even without the beamsplitter, the chances of coincidences are relatively low, as the detection efficiency of the single photon detectors is below 50% meaning that often only one photon of a pair will be detected.

III. QUANTUM OPTICS ADD-ON TOOLKITS

Following additional toolkits work only in conjunction with QOC.

A. QOA1-Single Photon Double Slit Experiment: Demonstrating the wave nature exhibited even by single photons

Apart from Michelson Interferometry, there is a second well-known experiment used to demonstrate how single photons can "interfere with themselves", the double slit experiment. In its classical configuration light is sent through a narrow double slit and the light that is diffracted at the individual slits results in an interference pattern on a screen at some distance from the double slit. In the case of single photons, one could naively assume that the photons either go through one slit or the other, rendering interference impossible. However, similar to the Michelson interferometer, the state of the photon after the double slit is a superposition of passing through slit-1 and slit-2, and tracking the position of a large number of single photons on the screen (in this case a detector) again reveals an interference pattern. This holds as long as the slits are indistinguishable. The interference can be destroyed by, for example, introducing polarizers in front of the two single slits that are perpendicular to each other. This is equivalent to the quantum erasure experiment in the Michelson interferometer. Introducing a 45° oriented polarizer behind the double slit would again erase the path information and retrieve the interference pattern.

Theory: The double slit interference pattern for classical light is well described by classical light wave theory. However, employing a quantum mechanical formulation for single photons yields the same result [17]. The pattern consists of a sinusoidal interference with a period depending on the distance between the two slits, and a sinc-shaped envelope with a period depending on the width of the individual slits. The period of both the interference and the envelope additionally depends on the distance between the double slit and the screen. Note that this is based on the assumption that the light incident on the double slit is spatially coherent, such as light coming from an ideal point source. This will not be the case in real-life experiments. In a simplified argument, a finite light source will result in different angles of incidence on the double slit depending on the source position. Each of those angles creates its own pattern on the screen, with the individual patterns being shifted in relation to each other, which will wash out the interference pattern. Assuming a finite light source with a Gaussian profile (a good approximation for the pump laser on the BBO crystal), one can use the von-Cittert-Zernicke theorem to calculate the so-called degree of spatial coherence $\gamma = \exp((\pi DS/\lambda Z)^2)$ where D is the separation of the slits (center-to-center) (see Fig. 15), S is the beam waist of the Gaussian light source, and Z is the distance between the source and the double slit. In the extreme case of completely destroyed coherence ($\gamma = 0$), only the envelope term remains, while for ideal coherence ($\gamma = 1$) we obtain full fringe visibility. Then it can be shown that

$$R(x) = \frac{2R_m}{1+\gamma}\left(\frac{\sin(C_{ss}x)}{C_{ss}x}\right)^2\frac{1}{2}(1+\gamma\cos(C_{ds}x)) \quad (12)$$

where $C_{ss} = \pi W/(\lambda L)$, $C_{ds} = 2\pi D/(\lambda L)$, $R(x)$ is the rate of photons at a specific screen position x, R_m is the maximum rate (considering all screen positions), W is the width of an individual slit, λ is the wavelength of the light, and L is the distance between double slit and screen, as shown in Fig. 15. A theoretical plot of $R(x)$ with parameter values $R_m = 100Hz, W = 100\mu m, D =$

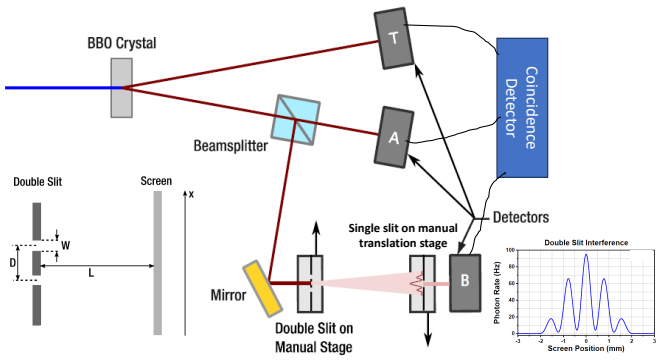

FIG. 15. Schematic of the single photons double slit experiment

$300\mu m, \lambda = 810nm, L = 30cm$ is shown in Fig. 15.

Setup: The fundamental setup is that of the GRA experiment (see Sec. II D). Other configurations, e.g., based on different dimensions of the double slit, are certainly possible. A mirror is introduced into the path from the beamsplitter to detector B, deflecting the beam towards the right breadboard edge (see Fig. 15). The light then falls on a double slit, generating the pattern described above. The mirror allows a longer distance between crystal and double slit, improving spatial coherence as described above. The double slit is placed on a manual translation stage to allow fine positioning.

As the detector has limited spatial resolution, the pattern cannot be recorded in a single measurement and instead has to be scanned. This is realized by introducing a single slit in the light path behind the double slit, which is mounted on a translation stage and can thus be moved in a perpendicular direction along the fringe pattern in small precise steps. The single slit plane corresponds to the screen plane in the equations above. The light that falls through the single slit is analyzed by detector B. As the optics of the detector are optimized to focus all incident light on the detector chip, the detector does not have to be moved along with the single slit but can remain at a static position. Furthermore, due to the very small distance between single slit and focusing lens of the detector the diffraction effects of the single slit itself can be neglected, as all light that passes through the slit ends up on the detector chip.

Measurement: The result of a measurement should look similar to the theoretical plot shown in Fig. 15. You can see the typical double slit pattern with an interference and an envelope. Please note that g2(0) value should be clearly below 1 in the region of the pattern, there by indicating single photon character for all significant data points. The exact amount of side maxima and their spacing depends on the double slit that is used as well as on the setup geometry. The parameters used for the calculated patterns in Fig. 15 correspond to the setup as described here.

Sample experimental measurement readings:

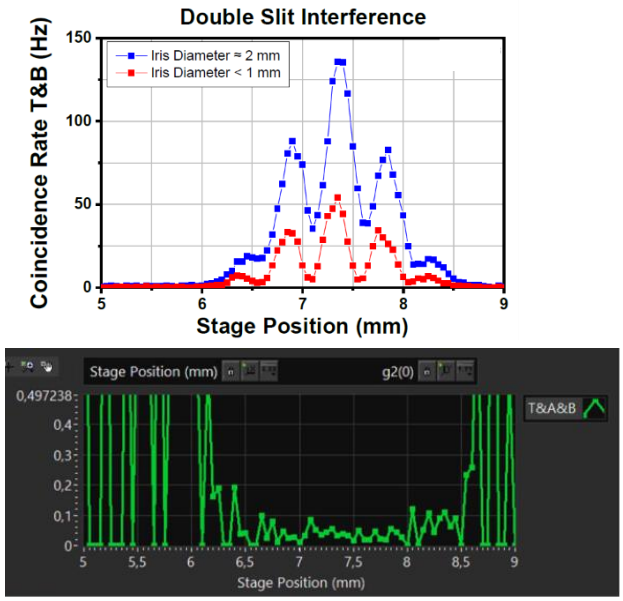

FIG. 16. Sample experimental measurement readings (taken from elsewhere) of the single photon double slit experiment. The simultaneously measured correlation values $g^{(2)}_{GRA}(0)$ are always well below 1 (in the region corresponding to principal and secondary maxima in the top plot), showing that the experiments were always performed in the single photon regime.

See Fig. 16.

The degree of coherence depends mainly on the diameter of the pump laser spot on the BBO crystal (light source size) and the distance between the crystal and the double slit. Increasing the latter is cumbersome in the confines of the current setup and comes with the disadvantage of even lower count rates due to divergence of the light. However closing the iris in front of the BBO crystal (and thus reducing the size of the light source) may prove to be the better way of increasing the coherence, even though it may also result in a decrease of the final count rates (less pump power on the crystal).

Changing the position of the double slit via the manual translation stage has no influence on the shape of the pattern but increases/decreases the overall count rates. The optimal slit position can be obtained via a measurement series of different slit positions. We recommend steps of 450 μm (three full rotations of the differential screw).

Sometimes the pattern is asymmetric. This is caused by the light hitting the double slit at a small angle. To achieve a symmetric pattern, rotate the lower kinematic screw of the mirror in front of the double slit with care. Clockwise rotation increases the right side-lobe and decreases the left one, while counterclockwise rotation of the screw has the opposite effect.

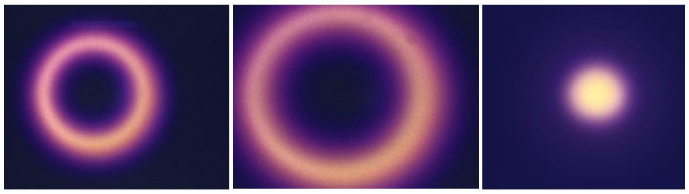

FIG. 17. The expected SPDC Cone Image with Camera for Phase Matching Conditions of the Experiments in this toolKit (Left), and for Tilted Crystal Resulting in Larger Opening Angles (Center) or Collinear Emission (Right). These images are shown here with a false color scale to increase visibility.

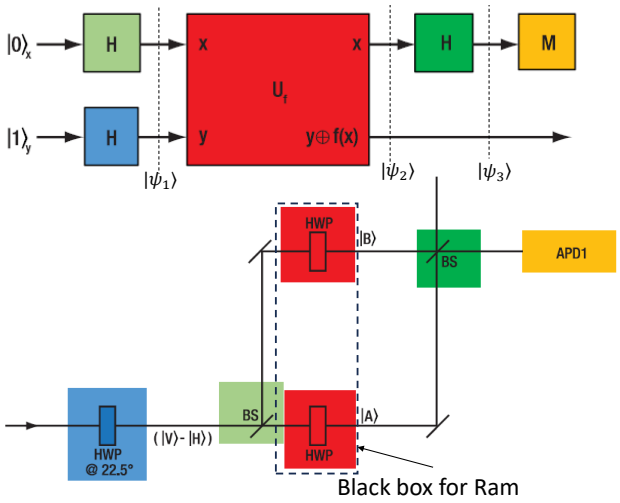

FIG. 18. Quantum circuit for the Deutsch algorithm (top) and schematic of the setup to realize the same optically in a Mach-Zehnder interferometer configuration (bottom) [20]. Here the two beam splitters are 50:50 and non-polarizing.

B. QOA2-Imaging the SPDC cone with a camera: Demonstrating momentum conservation and spatial correlation of single-photon pairs

By placing a camera, such as CS165MU, right behind the BBO crystal, it is possible to obtain direct images of the photons generated by the SPDC process. In order to eliminate the pump light from the images, one of the bandpass filters in the detector optics should be inserted between the crystal and camera. As the camera needs to be very close to the crystal to view the full cone without additional optics, we recommend turning the crystal mount by 180° for this exercise (so that the kinematic screws are not blocking the camera). The image quality can be increased by setting the pump laser to the maximum current of the diode. In this configuration, one can directly examine the influence of the phase matching conditions on the SPDC cone. Rotating the crystal around its vertical axis will increase or decrease the opening angle of the cone and hence the radius of the circle in the camera image, see Fig 17.

By increasing the gain of the camera, the required integration time can be reduced to the point of a low-framerate video, imaging the above-mentioned changes in real-time.

C. QOA3-Experiments with different BBO crystal thicknesses: Relation between intensity of single photons and crystal thickness

The thickness of the pair generation crystal influences the count rates. For a constant pump intensity, the single detector count rates are expected to scale approximately with the square of the crystal thickness. Furthermore, the spectral distribution of the photon pairs will vary depending on the thickness.

D. QOA4-Quantum computing: Demonstrating the Deutsch algorithm

Given an n-bit binary function $f : \{0,1\}^n \rightarrow \{0,1\}$, the Deutsch-Jozsa algorithm is designed to determine whether the function f is constant (same output for any input) or balanced (half of the inputs are mapped to 0 and the other half to 1). In the following we only consider the case for $n = 1$ (also known as the Deutsch algorithm), which can be solved by a two-qubit quantum computer in one run (see Fig. 18), while a classical computer would need to evaluate both $f(0)$ and $f(1)$ using two function calls [19, 20].

A simple analogy that may be used to describe the benefits of the Deutsch algorithm is that of a coin test: If Ram wants to know if Seetha is using a standard coin (one side heads and one side tails) or a fake coin (both sides heads or both sides tails) for their game of coin flips, Ram need two measurements in the classical case viz., look at one side of the coin and then look at the other side to see if it is the same or different. With the Deutsch algorithm, Ram only need to look at the coin once to know if it is standard or fake.

In the optical implementation of Deutsch algorithm, the first qubit is encoded in the photon path, namely, the two spatial modes A and B. In a dual-rail representation, the logical state $|0\rangle$ ($|1\rangle$) is associated with the physical state $|A\rangle$ ($|B\rangle$) which corresponds to the situation "one photon in mode A (B)" [20]. The second qubit is implemented via the photon's polarization states $|V\rangle, |H\rangle$ and the logical state $|0\rangle$ ($|1\rangle$) is associated with the physical state $|V\rangle$ ($|H\rangle$) [20].

The state of the two qubits after the two Hadamard gates is given by

$$|\psi_1\rangle = \frac{1}{2}(|A\rangle + |B\rangle)_x \otimes (|V\rangle - |H\rangle)_y \tag{13}$$

Note that the Hadamard gate H is nothing but a 90° rotation about positive y-axis in the Bloch sphere representation of a qubit [19].

The two-qubit gate $U_f(|x\rangle \otimes |y\rangle) = |x\rangle \otimes |y \oplus f(x)\rangle$ flips the state of the second qubit based on the defined function value for the first qubit's state and can be simply realized by controlled-NOT (C-NOT) gate. Here $\oplus$ is the modulo two operation. After this operation the two-qubit state is given by:

$$U_f|\psi_1\rangle = |\psi_2\rangle$$
$$= \pm\frac{1}{2}((-1)^{f(A)}|A\rangle + (-1)^{f(B)}|B\rangle)_x \otimes (|V\rangle - |H\rangle)_y \tag{14}$$

Note that due to the properties of the chosen input superposition state, the resulting y-qubit state remains identical to the input, while the information about the solution is imprinted onto the x-qubit via a process called phase-kickback (this in turn avoids entanglement between the two qubits but this is not an entanglement-free measurement of the qubit state because here we are extracting the information encoded in U_f but not in the qubit state). Here U_f is realized by selectively adding a half wave plate (HWP) (with its optic axis perpendicular to $(|V\rangle - |H\rangle)/\sqrt{2}$) to each spatial mode. In this case, HWP introduces a phase shift to the state of the y-qubit depending on the state of the x-qubit, as follows.

Let $|\pm\rangle_y = (|V\rangle \pm |H\rangle)_y/\sqrt{2}$. The optic axis is a direction in the crystal (HWP) along which light experiences no birefringence (the ordinary and extraordinary rays travel at the same speed). Action of HWP is as follows: Let the optic axis of the HWP be along $|V\rangle$. If the state of y-qubit incident on the HWP is $|H\rangle, |V\rangle, |+\rangle, |-\rangle$ then the state of y-qubit after HWP will be $(-|H\rangle), |V\rangle, |-\rangle, |+\rangle$ respectively.

A HWP can be used to define a range of different gates, for example: 1. If the HWP is oriented with its optic axis at 45° to the vertical axis ($|V\rangle$), it flips a photon with vertical polarization to horizontal polarization upon transmission, $|V\rangle \leftrightarrow |H\rangle$. This is a NOT gate, also known as an X-gate.

2. If the HWP is oriented with its optic axis at 22.5^o to the vertical axis, the photon is projected onto the polarization states $|V\rangle \rightarrow |+\rangle$ and $|H\rangle \rightarrow |-\rangle$ which corresponds to the definition of the Hadamard gate.

3. If the HWP is oriented with its optic axis along $|V\rangle$, it introduces a 180° phase shift to the $|H\rangle$. This is a phase gate (P-gate).

Note that if the optic axis of the HWP is set e.g., at 45° to the polarization direction of y-qubit state incident on the HWP (present in only one of the two paths A and B) after the first beam splitter, then there will be entanglement between the two qubits. Hence selectively applying HWP introduces the necessary coupling between path and polarization degrees of freedom of photon which in turn is capable of entangling the two qubits.

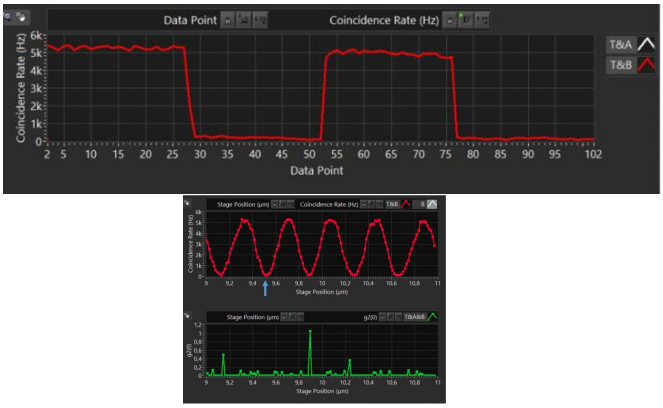

FIG. 19. Top: Sample experimental measurement readings (taken from elsewhere) of the realisation of the Deutsch algorithm using single photon qubits. Here constant (balanced) function corresponds to Minimum (maximum) T&B coincidence count rate. Bottom: The working point (shown by blue arrow) corresponds to a simultaneously measured correlation value $g^{(2)}_{GRA}(0) \ll 1$, there by ensuring that all further experiments were performed in the single photon regime.

The four possible setups represent the functions $f(A) = f(B)$ (constant functions) and $f(A) \neq f(B)$ (balanced functions), corresponding to two equal- and two different-sided coins, respectively. The transformation corresponding to U_f will be achieved if the value $f(x) = 1$ is assigned to "wave plate installed in arm $x \in \{A, B\}$" and the value $f(x) = 0$ to "no wave plate in arm x".

Recombining the two interferometer arms on a second non-polarizing 50:50 beam splitter implements a final Hadamard gate on the first qubit, yielding the final state:

$$|\psi_3\rangle = \begin{cases} \pm\frac{1}{\sqrt{2}}|B\rangle_x \otimes (|V\rangle - |H\rangle)_y \ (constant) \\ \pm\frac{1}{\sqrt{2}}|A\rangle_x \otimes (|V\rangle - |H\rangle)_y \ (balanced). \end{cases} \tag{15}$$

The experimental setup resembles a classical Mach-Zehnder interferometer (Fig. 18). Constructive (destructive) interference in the extension of mode A indicates a balanced (constant) function, i.e., one and only one wave plate (two or none wave plates) in the beam paths. The quantum character of our computation becomes obvious by the fact that it uses single-particle interference and that, in principle, a single detection event is sufficient to test the oracle function [20].

Sample experimental measurement readings: See Fig. 19.

E. QOA5-Demonstrating quantum entanglement/nonlocality via the violation of Bell-CHSH inequality: Motivation to quantum communication viz., QKD, quantum teleportation, likely possibility of superluminal communication etc.

Using QOC + QOA5 students can perform the following experiments. Schematic of the general setup for the experiments in QOA5 is described in Fig. 20 (a).

1. *Coincidence Rates at Polarizers - Unentangled Mixed-State*

Exercise: Measure the average coincidence count rates of each of the states of a mixed state ensemble of photon pairs in order to simulate a mixed state. The individual states of the mixed state can be produced by alternatingly pumping the SPDC process in only one of the crystals of the pair at a time. Observe how the coincidence count rates are influenced by the polarizers in front of the detectors, when both are turned from $0^o - 90^o$ in parallel.

Goal: Classical example: Observe the behavior of photon pairs at a pair of polarizers for a mixed state. Here, both horizontally and vertically polarized pair contributions follow Malus law.

Setup: The setup procedure for the entangled source is described in Fig. 20 (a). As we only pump one of the crystals in the crossed BBO pair to generate one of the photon pair polarizations at a time, the birefringent compensation crystals have no effect.

Measurement: For the ensemble result we will sum up the counts from both pair polarizations for each of the polarizer settings that contribute to the mixed state, so it does not matter in which order we generate and measure the HH-states and VV-states. To speed up the process, it is advisable to set the pump half-waveplate to 0° first (vertically polarized pump beam; horizontal photon pair polarization) and measure the coincidence count rate at about eight different settings of the detector polarizers between -20° *to* 100° (both polarizers should show the same rotation angles). Afterwards, repeat the measurements with the pump half-waveplate set to 45° (horizontally polarized pump beam; vertical photon pair polarization) with identical polarizer angles as before.

Interpretation: This mixed state is an example of an ensemble of states that contains similar large amounts of photon pairs polarized along the horizontal or vertical axis. As per the design of our experiment, we only generate one of the two polarizations at a time, and we know which one is generated. Therefore, there is neither superposition of states nor entanglement present in the density operator used to describe the ensemble of states we produced. The sums of the coincidence count rates for each of the polarizer settings that generate the HH-state and VV-state. To fit the model to the measured data, the horizontal and vertical polarization contributions should be weighted by the measured coincidence count rates at 0° *and* 90°. At 45° detector polarizer orientations, we observe a minimum of the curve at half the maximum coincidence count rate, as, according to Malus law, the probability for both a horizontally or vertically polarized photon to pass through each individual polarizer in each arm is equal to 1/2 and the probability for the pair to pass in coincidence is the product thereof (1/4). In contrast, at the maximum points of the curve at 0° *and* 90° the chance for either the horizontal or vertical polarizations to pass in each arm is equal to 1, but the respective other half of the photons (vertical or horizontal polarization) is blocked completely, such that we only detect half of the generated photons pair - but still twice as many as at the minimum.

Note that mixed states described by density matrices do not carry all the information about a quantum system and hence the density matrix description is not a complete description of a quantum system. The complete description of a quantum system is given by the state-vector/wave-function formalism. For further details see [15, 16].

2. *Coincidence Rates at Polarizers - Entangled Pure-State*

Exercise: Repeat the previous experiment with the entangled Bell state and compare your results.

Goal: Observe the different behavior of states generated by the entangled pair source.

Setup: The setup procedure for the entangled source is described in Fig. 20 (a).

Measurement: Here only one measurement is required for each polarizer angle, as the entangled pair source produces photon pairs with both polarization components. Apart from that, the measurement process is the same: Use the Malus law to record the coincidence count rates for about eight different detector polarizers settings between -20° *to* 100° (both polarizers always show the same rotation angle).

Interpretation: In contrast to the minima in the curve for the mixed state, the polarization-dependent coincidence count rates from the entangled state constantly are at a similar level as the maxima in the mixed state curve and, thus we obtain corresponding probability to be 1/2. For the cases of 0° *and* 90° orientation of the polarizers, we may use the same explanation as before: Only half of the generated photon pairs will pass through the polarizers, which are the ones with matching horizontal or vertical polarization. For any other polarizer setting, however, the above arguments do not hold up anymore and we observe higher coincidence rates than for the mixed state.

Outside of the 0° *and* 90° polarizer settings, we cannot tell the origin of the photon pair with certainty. Therefore, the polarization states of the single photons are not definable (however, the two-photon state is well defined). The moment one of the photons is "measured" by the

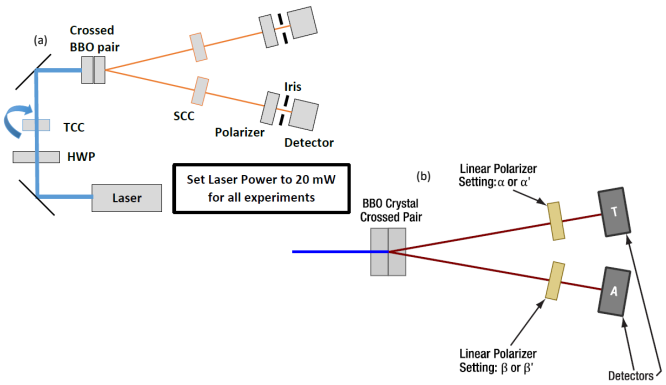

FIG. 20. (a) Schematic of the general setup used in QOA5 (TCC/SCC: Temporal/Spatial Compensation Crystals, HWP: Half-Wave Plate). (b) Schematic of the experimental setup to demonstrate violation of Bell-CHSH inequality.

polarizer (i.e., pass or block – both have the same probability of 1/2), the state of the other photon in the pair is determined by the result of the measurement. The Bell state $|\psi\rangle = (|H\rangle|H\rangle + |V\rangle|V\rangle)$ in this example leads to both photons being polarized along the same direction, thus they either both pass through or both get blocked by the polarizers in both arms equally.

Furthermore, this result also explains the alignment process used to set up the entangled pair source. During the step that adjusts the entangled state phase, the polarizers in front of both detectors are oriented in a crossed configuration. If the entangled state phase is adjusted for the $|\psi\rangle$ Bell state, both photons of a pair will have the same polarization orientation, but can only pass through one of the polarizers, while being blocked at the other one, resulting in a coincidence rate of zero (in the idealized case).

3. *Bell-CHSH test with polarization entangled photons*

The version of the Bell-CHSH (Clauser Horne Shimony Holt) inequality we use in this toolkit is based on the experimental setup shown in Fig. 20 (b). A source is emitting pairs of polarization-entangled photons with the photons being sent in different directions. In each arm, there is a linear polarizer, either transmitting or absorbing incident photons depending on the photon's polarization and the polarizer angle setting. One detector in each arm registers the transmitted photons.

Consider the two-photon polarization-entangled state

$$|\psi\rangle = \frac{1}{\sqrt{2}}(|H\rangle_1 \otimes |H\rangle_2 + |V\rangle_1 \otimes |V\rangle_2). \tag{16}$$

The idea behind Bell inequality is to show that the correlations between certain observables corresponding to the state $|\psi\rangle$ are in fact stronger than what can be explained by any local hidden variable theory based on causality (these theories are based on the assumption that information cannot be transmitted from one point in space to other at a speed greater than that of light, and this in turn leads to causality concept as can be seen from Einstein's special theory of relativity) [13]. One way to infer the expected correlations experimentally is by observing the probabilities of both photons in the state $|\psi\rangle$ to be transmitted as a function of the polarizer settings (here in the quantum case, the probability distribution corresponding to one photon depends on that of the other photon, independent of the spatial separation between them i.e., the two entangled photons are correlated in a nonlocal fashion). These probabilities can be measured in the experiment in Fig. 20 (b) via the coincidence rates of the detectors. CHSH defines specific relations (called the E-parameter) of these coincidence rates as follows:

$$E(\alpha,\beta) = \frac{R(\alpha,\beta) - R(\alpha,\beta+90^o) - R(\alpha+90^o,\beta) + R(\alpha+90^o,\beta+90^o)}{R(\alpha,\beta) + R(\alpha,\beta+90^o) + R(\alpha+90^o,\beta) + R(\alpha+90^o,\beta+90^o)} \tag{17}$$

where $R(\alpha,\beta)$ is the T&A coincidence count rate corresponding to the analyzer setting angles α,β. Using four E-parameters for four different experimental settings (analyzer angles), the following quantity is defined

$$S(\alpha,\alpha',\beta,\beta') = E(\alpha,\beta) + E(\alpha',\beta) + E(\alpha',\beta') - E(\alpha,\beta').$$

Bell-CHSH proved that, under the assumptions of locality and causality (more generally, noncontextual hidden variable (NCHV) assumption), all NCHV theories must obey the inequality:

$$S(\alpha,\alpha',\beta,\beta') \leq 2. \tag{18}$$

Note that in deriving this inequality, it is assumed that the two space-like separated photons are being measured simultaneously (clocks of Rama and Sita who are doing measurements on the photons, are synchronized as per special relativity). However quantum mechanics predicts that the quantity $S(\alpha = 0^o, \alpha' = 45^o, \beta = 22.5^o, \beta' = 67.5^o)$ measured on the state $|\psi\rangle$ must be $2\sqrt{2}$, and this is the maximum achievable value within standard quan-

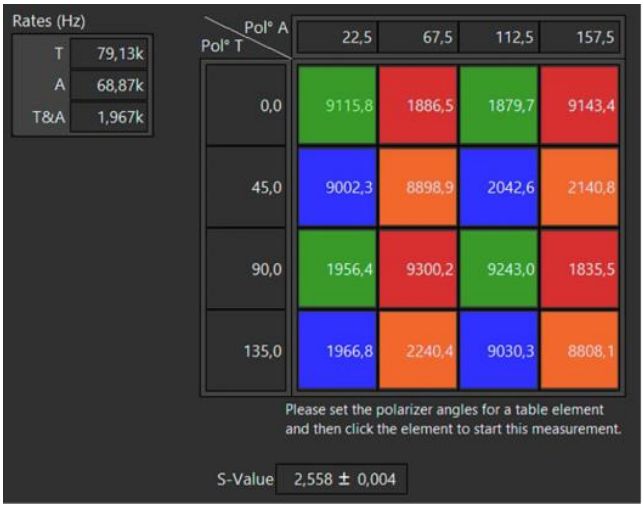

FIG. 21. Sample experimental measurement readings (taken from elsewhere) of the Bell-CHSH test using polarization entangled photons. Here the value ($R(\alpha,\beta)$) groups that go into the calculation of each parameter E are highlighted with the same colors. For example, values highlighted in green go into the calculation of $E(\alpha = 0^o, \beta = 90^o)$. Note that here no need to measure $g^{(2)}_{GRA}(0)$ to ensure that the experiments were performed with single photons. This is because the very fact that we obtain $S = 2.558$, itself confirms that the experiments were performed in the single photon regime (with mixed/classical states, we cannot obtain $S = 2.558$).

tum mechanics known as Tsirelson bound (note that the algebraic bound of S is 4). This shows that entangled particles can communicate in a nonlocal (i.e., instantaneous) fashion.

Sample experimental measurement readings: See Fig. 21.

Result and discussion: To close the locality loophole it is necessary to make the measurement events to be space-like separated (i.e., they should lie outside the light-cone and hence be causally disconnected). To achieve this, separate the two detectors in Fig. 20 by more than $30cm = c\delta t$ so that no information can be transmitted between the two detectors in a local fashion, where c is the speed of light and $\delta t \sim ns$ is the coincidence time window of the coincidence detector. And choose the polarizers angle settings in real time, simultaneously. For further details on this loophole-free test, see [12].

Likely possibility of superluminal communication: We showed that the two entangled photons are able to communicate superluminally (i.e., faster than the speed of light). Can we exploit these nonlocal correlations for superluminal communication? Yes, provided we can distinguish between two maximally mixed but physically different ensembles as proposed in [15, 16], or if we can measure a single unknown quantum state as proposed in [22] (also see Sec. III F). Note that these two are theoretical ideas which have not yet been verified experimentally.

4. *Changing the Phase of the Entangled State*

Exercise: In this exercise the phase of the entangled state is changed by tilting the temporal compensation crystal and the previous experiments are run again with the new state. This exercise is split into three subsections.

Goal: Understand the importance of the entangled state's phase for the Bell test and learn how to adjust it.

Setup: Start out from the previous experiment settings and set the polarizers in front of detectors T & A to $\pm 45^o$. Carefully tilt the temporal compensation crystal to change the phase delay between horizontal and vertical polarization. This effect can be observed in the coincidence count rate. For a quantitative analysis, one should use the Malus' law (as shown in the measurement below).

4.1 Adjusting the Phase

When both polarizers in front of the detectors are oriented along the 45° axis, the phase difference ϕ of the entangled state determines the expected result of the experiment. The probability of both photons passing the polarizers is given by

$$(1 + \cos\phi)/4 \tag{19}$$

and it can be as high as 0.5 (in the $\phi = 0$) and as low as 0 (for $\phi = 180^o$). It is thus important to know the phase difference when determining the expectation values for this kind of experiment.

Exercise: Tilt the temporal compensation crystal using the upper adjuster knob to change the phase of the entangled state and record coincidence count rate measurements with polarizers in front of detectors T & A set to $\pm 45^o$. Use the upper kinematic adjuster of the crystal mount and turn it 1/4 revolution per step (at least 10 steps).

Interpret the Results: How does the coincidence count rate change and why?

Measurement: Take the measurements of the coincidence rates for a range of tilt settings of the temporal compensation crystal (TCC) between 0° and 3° angle of incidence for the blue pump beam. The upper adjuster knob on the crystal mount should be turned by 1/4 revolution for each measurement along the same direction. The tilt angle is estimated from the specified 0.5^o tilt angle per revolution for this mount.

Result Analysis: The observed rates resemble the shape of a (shifted) sine function with respect to the tilt angle. Comparing to Eq. (19), we can explain the minima and maxima in our measurement result, which occur at $\phi = 0, \pi$ respectively (both modulo 2π; these are for shifted cosine i.e., sine function). As discussed earlier, the absolute phase ϕ between both polarizations depends on the exact thicknesses and orientations of all birefringent

elements in the beam paths and varies between every new alignment of the setup. The phase shift $\Delta\phi$ is generally not a linear function with respect to the tilt angle of the birefringent element used to tune the phase. The temporal compensation crystal used in the kit is designed to allow for multiple periods in the phase shift $\Delta\phi$ within the tilt range of a kinematic mount. In this small angular range, a linear approximation can be justified for this crystal.

The period of the oscillations is 1.2^o of TCC tilt angle change, in line with the theoretical calculations.

4.2 Coincidence Rates at Polarizers

Exercise: Turn the blue thumbscrew of the temporal compensation crystal in order to adjust the phase for a maximum coincidence rate at $\pm 45^o$ polarizer settings (this sets the state to $(|H\rangle \otimes |H\rangle - |V\rangle \otimes |V\rangle)$. Compare the coincidence count rates for both polarizers at 0° and both polarizers at 90° and adjust the HWP until both values are about the same. Do the same measurement as in previous experiment (use the Malus law again), but this time leave the TCC untouched and instead change both polarizer angles simultaneously (steps of 22.5^o). How does the coincidence rate depend on the polarizer settings when both polarizer angles are rotated with the same orientation (as earlier) or when the polarizer in front of detector A is always rotated in the opposite direction to the negative angle of the polarizer in front of detector T?

Measurement: After selecting the smallest TCC tilt angle with maximum coincidence count rate (0.2^o) from the measurement above, the following dependencies of the coincidence count rates with respect to the polarizer angles is measured. Note that there is a small imbalance between the horizontal and vertical pair production rate, as the fine alignment of the pump half-waveplate has not been adjusted after changing the angle of the birefringent TCC.

Result Analysis: The result when rotating both detector polarizers in parallel may be surprising at first, as the curve will be more similar to the one of the mixed state (Sec. III E 1), instead of the entangled state measured in Sec. III E 2. However, note that in this case the curve approaches zero in the 45° polarizer setting, which is not possible for the mixed state. With the changed phase of the entangled state, the polarizations measurable in both arms are now not parallel anymore - instead the second measurement confirms that the polarizations in both arms are now mirror-symmetric with respect to the center plane between the two detectors. With the polarizers at 45° orientations, the two arms' polarizations are orthogonal to each other.

Result-A: The coincidence probability for the entangled state is always 0.5, as long as the polarizers have the same setting, regardless of which setting that is. This coincidence probability of 50% irrespective of the angle setting of the identical polarizers cannot be explained with conventional classical physics. One would either have to introduce new hidden variables that affect the polarization measurements (even this approach fails when more setting combinations are taken into account) or propose that the measurement result of one photon affects the state of the other. For example, this result could be explained as follows: whatever polarization the first photon is measured to have, the second photon will instantly change its state to exactly this polarization. Or in other words: the two photons have individually undefined polarization, but they will always be measured to be in the same polarization state.

These results can be compared to result-A discussed in the previous paragraph where the changed phase leads to "-" signs instead of "+". To fit the models to data, weight the unbalanced contributions of horizontal and vertical state generation by the coincidence count rates measured at 0° *and* 90°:

$$R(\phi) = (\sqrt{R(0^o)}\cos^2\phi \pm \sqrt{R(90^o)}\sin^2\phi)^2. \qquad (20)$$

The version with "-" is used to fit the measurement with parallel polarizer orientations, whereas the "+" is used for measurements with mirror symmetric polarizer orientations. This is because, when one of the polarizer angles has flipped sign, then the "-" signs in result-A cancel and the result is probability = 0.5 for all angles again (in the idealized case of equal contribution of horizontal and vertical states).

4.3 Bell test:

Exercise: Repeat the Bell test at the current phase setting with maximal coincidence count rate at $\pm 45^o$ polarizer orientations. How can the result of the test be interpreted? Can the test itself or the evaluation equations be changed to adapt the test to the changed input state?

Measurement: Running the Bell test shows a "failed" result with S close to zero. Comparing to the result in Sec. III E 3, the order of results with high and low count rates is the same in the 0° and 90° settings but changed in the 45° *and* 135° settings.

Result Analysis: The S-value obtained with the default settings for the Bell test will be rather close to zero instead of breaking the limit of 2. The explanation of this result can be found by theoretically evaluating the Bell-CHSH term S for a $|x\rangle_1|x\rangle_2 - |y\rangle_1|y\rangle_2$ state and with arbitrary polarizer angles α, β and considering solely a change from the difference $\alpha - \beta$ in the arguments of the (co)sine functions towards $\alpha + \beta$ (and the variants with primed letters). However, the values we used for $\alpha, \alpha', \beta, \beta'$ now result in different values for the four E terms when evaluating S:

$$S_\phi(\alpha,\alpha',\beta,\beta') = \cos(2\alpha+2\beta) - \cos(2\alpha+2\beta') + \cos(2\alpha'+2\beta) + \cos(2\alpha'+2\beta') \quad (21)$$
$$= \cos(2\times 22.5^o) - \cos(2\times 67.5^o) + \cos(2\times 67.5^o) + \cos(2\times 112.5^o) = 0. \quad (22)$$

Thus, this setting is not suitable to violate the CHSH inequality and other parameters are required. Considering that we changed the sign of the angle of one of the polarizers during alignment to set this Bell state, it is easy to motivate just changing the sign for all the angles in the Bell test of one of the polarizers. This assumption can be further justified, as we look at the mathematical derivation again. We noticed earlier that, with the $|x\rangle_1|x\rangle_2 - |y\rangle_1|y\rangle_2$ state, we get $\alpha+\beta$ for all the effective angles involved for the evaluation of S and we need to find a new set of angles to obtain a maximum value of S. On the other hand, we already know that our previous set of angles with the term $\alpha-\beta$ is a desired solution. Therefore, inverting the sign of all our angles β,β' must then also yield a desired solution for this Bell state. The same holds true for inverting only the α,α' angles, as $\cos(2\theta)$ is symmetric under inversion of sign.

Alternatively, we may change the definition of S: By shifting the minus sign in the equation from the α,β' term to the α,β term, we end up with another asymmetric equation, yielding the same type of inequality as before. However, when still using the default angles with positive sign, this changes the first two signs in the evaluation of S above:

$$S = |-(1/\sqrt{2}) + (-1/\sqrt{2}) + (-1/\sqrt{2}) + (-1/\sqrt{2})| = 2\sqrt{2}$$

Plugging in our measured values above into this changed equation, we should obtain the value of S well above the limit of 2 and fully in line with the result obtained earlier.

Interpretation: It is possible to reformulate the Bell-CHSH inequality also with other Bell states than considered earlier. However, a single formulation of the Bell test together with a certain choice of test angles is always directly linked to a certain Bell state, i.e., Bell tests are generally not universal. Thus, the result of the Bell test is also an indicator of how well the matching Bell state has been generated.

5. *Changing the Detector Iris Apertures*

Exercise: Compare the results of the Bell test when the aperture diameter of the irises in front of the detectors are reduced equally. Interpret the resulting curve.

Goal: Observe, how the detector iris apertures affect the measurement result.

Setup: Set up the experiment as earlier. Repeat the Bell test for 2-3 different iris aperture diameters between 3 to 10 mm in front of the detector pair. To reduce errors in the iris aperture diameter measurement due to backlash, it is advisable to close the irises to 1 mm and only monotonously increase the opening diameter from 3 to 10 mm during the measurement series.

Measurement: Here, the S-value of the Bell test is similarly high for all measurements, but slightly increases with smaller iris diameters. It violates the Bell-CHSH inequality for all iris diameters.

Interpretation: The S-value of the Bell test only reaches Tsirelson's bound of $2\sqrt{2}$ for optimally prepared Bell states and is one indicator of how well the Bell state has been prepared. As discussed earlier, the generation of photon pairs is subject to walk-off, which needs to be compensated. The measurements above indicate that our walk-off compensation is not perfect: Because we average over a smaller collection area, the phase range due to spatial walk-off decreases with smaller iris diameters, thus improving the quality of the detected Bell states. Extrapolating to zero diameter, i.e., simulating the collection at a single point in space without negative effects of spatial walk-off, shows that the optimal S-value still cannot be reached. This may be an indicator that there still is temporal walk-off or other effects that reduce the Bell state quality. Note however, that the extrapolation is to be taken with care, as a linear approximation of the curve cannot be justified in all cases. Compare this result to the result: the broadening of the entangled state phase distribution is generally not a linear function with respect to the iris aperture diameter. Instead, the phase maps are curved surfaces.

6. *Spatial Compensators*

Exercise: Remove the spatial compensation crystals from the setup. Now again, compare the results of the Bell test when the aperture diameter of the irises in front of the detectors are changed equally. Interpret the change of the slope of the curve in comparison to the previous experiment.

Goal: Understand the importance of spatial compensation and the interplay with detector iris aperture.

Setup: Set up the experiment as earlier, but remove the spatial compensation crystals from the beam path before aligning the phase of the entangled state (higher count rates at the minima than before are expected).

Note: It is further possible to remove just one of the spatial compensation crystals. Again, adjust the phase properly before the measurement. In this case, the obtained result will then be about half-way between the full compensated and uncompensated result.

Measurement: Here, the S-value of the Bell test significantly decreases with larger iris diameters. The violation of the CHSH inequality cannot be shown for all iris diameters.

Interpretation: Without the spatial compensation

crystals, the S-value and thus the quality of the Bell state drop off much faster with increasing iris diameter than for a properly compensated source. Due to the large spatial walk-off present in the crossed BBO crystal pair, the phase distribution for the pairs of entangled photons is so broad, when collected over large iris diameters, that the measured two-photon state is closer to a separable state instead of a Bell state. The effect is strong enough to cause the S-value to drop below the limit of 2 for large iris diameters and the test then fails to violate the CHSH inequality. It does not mean that now Hidden Variable theories involving local realism would suddenly be allowed. Instead, we just failed to set up the Bell test under proper conditions.

The S-value significantly improves with smaller iris diameters, as we filter out a smaller subset of photon pairs with a narrower phase distribution, closer to the ideal Bell state. Seemingly, the S-value may always be improved by more restrictive spatial filtering. However, note that the coincidence count rates decrease rapidly with smaller iris diameters, which in turn increases the uncertainty of the measurement. Comparing with the fully spatially compensated result, we conclude that using spatial compensation allows the measurement of high S-values together with significantly higher count rates at large iris diameters. This compensation allows for lower uncertainties and/or shorter measurement times for the Bell test, easier alignment of the system and leaves enough room for loss of count rate due to alignment issues or additional optical elements for additional experiments. The S-value extrapolated towards zero iris aperture diameter is larger here without spatial compensation due to the polarization distorting effects being reinforced by the birefringent spatial compensation crystals; if the input polarization is not matching to the optical axes plane of the crystal, it can further enhance the distortion, as it acts similar to a wave plate as well. These kinds of effects vary from setup to setup. Also remember the note on the validity of the extrapolation from the previous section.

7. *Changing the Temporal Walk-Off Compensation*

Exercise: Compare the results of the Bell test without temporal walk-off compensation and with increased walk-off. Interpret the results. Can the detector irises be used to mitigate effects of temporal walk-off, as before? Are there other measures to reduce temporal walk-off?

Goal: Understand the importance of temporal compensation.

Setup: Two configurations for the temporal compensation can be compared to the experiment in Sec. III E 3. Both require the spatial compensation crystals to be aligned in the beam path. Remember to adjust the half-waveplate for equal coincidence count rates in horizontal and vertical polarizer settings for both configurations.

1. Negative compensation: Rotate the temporal compensation crystal in its mount by 90°. Set up the experiment as earlier to align the phase of the entangled state, use the lower (black) kinematic screw of the temporal compensation crystal mount instead of the upper (blue) one. Remember to rotate the temporal compensation crystal back after this experiment section and realign its mount using the pump beam back reflection.

Bonus: Run the experiment again with the detector irises closed down to 4 mm.

2. No compensation: Set up the experiment as in Sec. III E 3, but remove the temporal compensation crystal from the beam path. To align the phase of the entangled state, use the lower kinematic screw of one of the spatial compensation crystal mounts. This is an exception for this configuration only. Remember to realign the spatial compensation crystal using the axicon after the experiment.

Measurement: Running the Bell test in the two configurations as described should yield the following results: Negative Compensation should result in an S-value significantly lower than measured before with the correct compensation. This value can even be below 2.

No compensation results in an S-value about halfway in between the values measured for correct compensation and negative compensation.

The Bonus measurement (negative compensation, 4 mm iris apertures) should result in an S-value similar to the negative compensation result.

Interpretation: Without the temporal compensation crystal, the S-value and thus the quality of the Bell state drop in comparison to the properly compensated configuration used in Sec. III E 3. Due to the finite spectral bandwidth of the pump laser, a range of different pump wavelengths may cause a photon pair generation in the SPDC process. As the birefringent refractive indices of the BBO crystals are dispersive, the photon pairs generated by different pump wavelengths acquire different phases on their way to the detector, which adds to the width of the phase distribution of the ensemble of entangled states and reduces the observability of entanglement effects.

In the usual orientation, the temporal compensation crystal pre-compensates this wavelength-dependent phase walk-off between both polarizations. Inserting the temporal compensation crystal in the "wrong" 90° rotated orientation flips the fast and slow axes of the birefringent crystal, which inverts the sign of the phase compensation and thus doubles the walk-off, instead of compensating it. When reducing the detector iris aperture, there is no significant improvement of the S-value. The measured increase of the S-value is similar to what can be observed in Sec. III E 5 and is due to the residual spatial walk-off still present in the system. This means that the temporal walk-off cannot be mitigated by smaller iris apertures, as it is not depending on the detection angle (i.e., spatial walk-off). The only alternative to reduce the effect of temporal walk-off is the reduction of the pump laser's spectral bandwidth, e.g. by using a single-frequency laser.

8. GRA Experiment for the Entangled Source (No Polarizers)

Exercise: Perform the Grangier-Roger-Aspect experiment for the entangled pair source. Does this source emit single photon pairs?

Goal: Understand that entanglement is NOT caused by two pairs (HH and VV) emitted at the same time, but by superposition of states of a single pair.

Setup: Remove the polarizers from the Bell test setup and add a beamsplitter and the third detector.

Measurement: Perform the GRA experiment.

Interpretation: The result is a value of $g^{(2)}_{GRA}(0)$ of 0.1 or lower. This proves that the entangled pair source emits single photon pairs, just as the source of the base kit. It thus becomes clear that the entanglement cannot be caused by HH and VV pairs being emitted simultaneously but that a single pair of photons is in a superposition of the HH and VV states. In this experiment, the polarizers were removed. Re-introducing them can only absorb photons, not create any new ones, so the single-pair character of the source remains intact and does not depend on the polarizer settings in any way.

F. QOA6-Testing a new interpretation of quantum mechanics: Exploring quantum foundations

A new interpretation of quantum mechanics viz., nonlocal-hopping particle interpretation (NPI), tries to unite the wave-particle dual natures exhibited by a quantum object using the concept of quantum nonlocality [22]. Some preliminary tests of NPI may be performed using QOC + QOA6, as described in [22] (supplementary material). If NPI is verified experimentally, then it will have profound implications on both technology (e.g., measuring a single unknown quantum state which in turn leads to superluminal communication) and also on our fundamental understanding of the nature. For further details see [22].

IV. SETTING UP THE TOOLKITS

Temperature Dependence of Pump Laser Wavelength: The center wavelength of the laser diode depends on the temperature. The wavelength increases linearly with temperature and the coefficient is about 0.05 nmK. This means that the wavelength can be tuned by 0.5 nm over the full temperature range of the diode mount (this has integrated TEC to vary temperature from 20-30 deg C). Please note that the diode temperature is influenced not only by the set point of the controller, but also by the laser current. A higher current increases the temperature and therefore leads to slightly longer wavelength at the same controller set point. Vice versa, a change in temperature can change the output power at the same current. Increase the laser current until the laser threshold is surpassed (brightness of the spot increases sharply).

The FPGA based coincidence counter can be interfaced with a computer (for data collection and analysis, and for controlling the experiments) using a software like LabView or MyOpenLab (open source) etc. It is also possible to program the FPGA directly in which case no need to interface it with a computer.

V. INTRODUCTION TO QUANTUM MECHANICS

A. Linear Algebra

B. Postulates of quantum mechanics

De-Broglie relation. Wave-particle duality. Bohr's complementarity principle.

VI. INTRODUCTION TO QUANTUM ELECTRODYNAMICS

A. Classical light: Maxwell's equations

B. Quantum light: Quantize classical light/field - Klein-Gordan equation and Single photons

VII. BASICS OF QUANTUM INFORMATION AND QUANTUM COMPUTING

Pure states and mixed states. Unitary quantum gates. Bloch sphere representation of a qubit state.

A. Quantum nonlocality and Bell-CHSH inequality

Ram (Sita) randomly measures one of the two dichotomic observables Q, R (T, V) with eigenvalues $q = \pm 1, r = \pm 1$ ($t = \pm 1, v = \pm 1$) respectively, on his (her) qubit. According to NCHV theories, the values of the observables are preassigned and hence the quantity $S = (q + r)t + (r - q)v = \pm 2$. However as per quantum contextuality, if T and V do not commute, then the outcome of measuring Q on maximally entangled two-qubit state, depends on whether it is measured in the context of T or V. Similar context dependency holds for R, T and V as well. This in turn leads to $S = 2\sqrt{2}$ with maximally entangled states and noncommuting observables (Q,R) and (T,V).

[1] Frank Arute et. al. Quantum supremacy using a programmable superconducting processor. *Nature*, 574:505, 2019.

[2] S. Bandyopadhyay. Welcher weg experiments, duality and the orthodox bohr's complementarity principle. *Physics Letters A*, 276(5):233–239, 2000. ISSN 0375-9601. doi:https://doi.org/10.1016/S0375-9601(00)00670-8. URL https://www.sciencedirect.com/science/article/pii/S0375960100006708.

[3] M. Beck. *Quantum Mechanics, Theory and Experiment*. Oxford University Press, Oxford, 2012.

[4] S Bize, P Laurent, M Abgrall, H Marion, I Maksimovic, L Cacciapuoti, J Grünert, C Vian, F Pereira dos Santos, P Rosenbusch, P Lemonde, G Santarelli, P Wolf, A Clairon, A Luiten, M Tobar, and C Salomon. Cold atom clocks and applications. *Journal of Physics B: Atomic, Molecular and Optical Physics*, 38(9): S449, apr 2005. doi:10.1088/0953-4075/38/9/002. URL https://dx.doi.org/10.1088/0953-4075/38/9/002.

[5] Joseph M Brom and Frank Rioux. Polarized light and quantum mechanics: An optical analog of the stern–gerlach experiment. *The Chemical Educator*, 7:200–204, 2002. URL https://doi.org/10.1007/s00897020580a.

[6] R. HANBURY BROWN and R. Q. TWISS. Correlation between photons in two coherent beams of light. *Nature*, 177:27–29, 1956.

[7] Stephan Dürr and Gerhard Rempe. Can wave–particle duality be based on the uncertainty relation? *American Journal of Physics*, 68(11):1021–1024, 2000. doi: 10.1119/1.1285869. URL https://doi.org/10.1119/1.1285869.

[8] A. Einstein, B. Podolsky, and N. Rosen. Can quantum-mechanical description of physical reality be considered complete? *Phys. Rev.*, 47:777–780, May 1935. doi: 10.1103/PhysRev.47.777. URL http://link.aps.org/doi/10.1103/PhysRev.47.777.

[9] E. J. Galvez, Charles H. Holbrow, M. J. Pysher, J. W. Martin, N. Courtemanche, L. Heilig, and J. Spencer. Interference with correlated photons: Five quantum mechanics experiments for undergraduates. *American Journal of Physics*, 73(2):127–140, 02 2005. ISSN 0002-9505. doi:10.1119/1.1796811.

[10] Remi Geiger, Arnaud Landragin, Sébastien Merlet, and Franck Pereira Dos Santos. High-accuracy inertial measurements with cold-atom sensors. *AVS Quantum Science*, 2(2):024702, 06 2020. ISSN 2639-0213. doi: 10.1116/5.0009093. URL https://doi.org/10.1116/5.0009093.

[11] Partha Ghose. Wave-particle duality: The mystery keeps unfolding. *Pramana-Journal of Physics*, 51:651, 1998.

[12] B Hensen, H Bernien, A E Dreau, A Reiserer, N Kalb, M S Blok, J Ruitenberg, R F L Vermeulen, R N Schouten, C Abellan, W Amaya, V Pruneri, M W Mitchell, M Markham, D J Twitchen, D Elkouss, S Wehner, T H Taminiau, and R Hanson. Loophole-free bell inequality violation using electron spins separated by 1.3 kilometres. *Nature*, 526(7575):682–686, October 2015. ISSN 0028-0836. doi:10.1038/nature15759. URL http://dx.doi.org/10.1038/nature15759.

[13] Dipankar Home. *Conceptual Foundations of Quantum Physics: An Overview from Modern Perspectives*. Springer Science and Business media, 1997.

[14] Y. Japha, O. Arzouan, Y. Avishai, and R. Folman. Using time-reversal symmetry for sensitive incoherent matter-wave sagnac interferometry. *Phys. Rev. Lett.*, 99:060402, Aug 2007. doi: 10.1103/PhysRevLett.99.060402. URL https://link.aps.org/doi/10.1103/PhysRevLett.99.060402.

[15] C S S Kumar, A Biswas, A Sen(De), and U Sen. Frequentist-approach inspired theory of quantum random phenomena predicts signaling. *arXiv:1903.12096v2 [quant-ph]*, Oct 2020.

[16] C. S. Sudheer Kumar. *Exploring quantum foundations by NMR: Quantum correlations and measurements*. PhD thesis, Indian Institute of Science Education and Research-Pune, 2021, (http://dr.iiserpune.ac.in:8080/xmlui/handle/123456789/5707). URL https://sites.iiserpune.ac.in/~mahesh.ts/thesis/Thesis5SudheerKumar.pdf.

[17] Bill J. Luo, Leia Francis, Valeria Rodríguez-Fajardo, Enrique J. Galvez, and Farbod Khoshnoud. Young's double-slit interference demonstration with single photons. *American Journal of Physics*, 92(4):308–316, 04 2024. ISSN 0002-9505. doi:10.1119/5.0179131. URL https://doi.org/10.1119/5.0179131.

[18] Karl-Peter Marzlin, Barry C. Sanders, and Peter L. Knight. Complementarity and uncertainty relations for matter-wave interferometry. *Phys. Rev. A*, 78: 062107, Dec 2008. doi:10.1103/PhysRevA.78.062107. URL https://link.aps.org/doi/10.1103/PhysRevA.78.062107.

[19] Michael A. Nielsen and Isaac L. Chuang. *Quantum Computation and Quantum Information*. Cambridge University Press, 2010. ISBN 9780511976667. URL http://dx.doi.org/10.1017/CBO9780511976667.

[20] M. Scholz, T. Aichele, S. Ramelow, and O. Benson. Deutsch-jozsa algorithm using triggered single photons from a single quantum dot. *Phys. Rev. Lett.*, 96:180501, May 2006. URL https://link.aps.org/doi/10.1103/PhysRevLett.96.180501.

[21] Maria Stromme. Universal consciousness as foundational field: A theoretical bridge between quantum physics and non-dual philosophy. *AIP Advances*, 15(11):115319, 11 2025. ISSN 2158-3226. doi:10.1063/5.0290984. URL https://doi.org/10.1063/5.0290984.

[22] C S Sudheer Kumar. Uniting the wave-particle dual natures via a nonlocal-hopping particle: Likely possibility of measuring a single unknown quantum state. *Precify Impex Private Limited - Bengaluru*, 2026. URL https://drive.google.com/drive/folders/1i3LPTv83cVbo8GpUZhjCx_23a7esF0oQ?usp=drive_link.

[23] Jamie Vovrosh, Andrei Dragomir, Ben Stray, and Daniel Boddice. Advances in portable atom interferometry-based gravity sensing. *Sensors*, 23(17):7651, 2023. ISSN 1424-8220. doi:10.3390/s23177651. URL https://www.mdpi.com/1424-8220/23/17/7651.